Draft version January 16, 2014
Preprint typeset using LaTeX style emulateapj v. 11/10/09

KINEMATIC EVOLUTION OF SIMULATED STAR-FORMING GALAXIES

Susan A. Kassin,[1] Alyson Brooks,[2] Fabio Governato,[3] Benjamin J. Weiner,[4] and Jonathan P. Gardner[5]

Draft version January 16, 2014

ABSTRACT

Recent observations have shown that star-forming galaxies like our own Milky Way evolve kinematically into ordered thin disks over the last ~ 8 billion years since $z = 1.2$, undergoing a process of "disk settling." For the first time, we study the kinematic evolution of a suite of four state of the art "zoom in" hydrodynamic simulations of galaxy formation and evolution in a fully cosmological context and compare with these observations. Until now, robust measurements of the internal kinematics of simulated galaxies were lacking as the simulations suffered from low resolution, overproduction of stars, and overly massive bulges. The current generation of simulations has made great progress in overcoming these difficulties and is ready for a kinematic analysis. We show that simulated galaxies follow the same kinematic trends as real galaxies: they progressively decrease in disordered motions (σ_g) and increase in ordered rotation (V_{rot}) with time. The slopes of the relations between both σ_g and V_{rot} with redshift are consistent between the simulations and the observations. In addition, the morphologies of the simulated galaxies become less disturbed with time, also consistent with observations. This match between the simulated and observed trends is a significant success for the current generation of simulations, and a first step in determining the physical processes behind disk settling.

Subject headings: galaxies – formation, galaxies – evolution, galaxies – kinematics and dynamics, galaxies – fundamental properties

1. INTRODUCTION

Over the last ~ 8 billion years since a redshift of one, the population of star-forming galaxies of ∼Milky Way mass has settled kinematically into flat, rotationally-supported, disk galaxies (Kassin et al. 2007, 2012). In the past, these galaxies had more disordered motions (as measured via an integrated gas velocity dispersion, σ_g) and less ordered rotation (V_{rot}) than they do today (Flores et al. 2006; Kassin et al. 2007; Vergani et al. 2012; Kassin et al. 2012). Over $0.1 < z < 1.2$, the median σ_g of star-forming galaxies of ∼Milky Way mass has progressively decreased while V_{rot} has increased (Kassin et al. 2012). Observations at even higher redshifts ($z \sim 1.5 - 3$), albeit where galaxy samples are much less representative, also find star-forming galaxies with large amounts of disordered motions, as measured through σ_g (e.g., Förster-Schreiber et al. 2009; Law et al. 2009; Wright et al. 2009; Lemoine-Busserolle & Lamareille 2010; Lemoine-Busserolle et al. 2010; Gnerucci et al. 2011).

These findings are an important benchmark for any theory or simulation of disk galaxy formation. Constraints on the internal kinematics of galaxies are significantly more stringent than constraints on e.g., luminosity, stellar mass, or star formation rate. Internal kinematics directly dictate how the gas in galaxies is arranged, which is heavily influenced by the physical processes involved in galaxy evolution. Furthermore, if theory is able to successfully reproduce observations of kinematic evolution, then it becomes a useful tool to help interpret the observations. In particular, we would like to know the physical processes behind disk settling.

Until now, robust measurements of the internal kinematics of simulated galaxies were lacking as the simulations suffered from low resolution, overproduction of stars, and overly massive bulges. These problems were ameliorated by increased resolution (e.g., Mayer et al. 2001), better treatment of feedback (Stinson et al. 2006; Hopkins et al. 2012; Wise et al. 2012), and modeling of the ultraviolet background (Quinn, Katz, & Efstathiou 1996). The current generation of galaxy simulations is able to match the rotation velocities, sizes, stellar masses, and baryon fractions of local disk galaxies (e.g., Governato et al. 2007; Brooks et al. 2011; Brook et al. 2012; Munshi et al. 2013; Christensen et al. 2013; Vogelsberger et al. 2013), as well as some properties of higher redshift galaxies (e.g., Hirschmann et al. 2013; Zemp et al. 2013; Hopkins et al. 2013). They are the first generation of simulations which are able to make quantitative predictions for the internal kinematics of galaxies.

However, most simulations have concentrated on reproducing only the rotation velocities of local disk galaxies (e.g., Guedes et al. 2011; Stinson et al. 2013; McCarthy et al. 2012; Brook et al. 2012). A few have measured σ_g, but only for $z = 0$ (e.g., Rôskar et al. 2013; Agertz et al. 2013) or $z = 2$ (e.g., Ceverino, Dekel, & Bournaud 2010; Anglés-Alcázar et al. 2013). Croft et al. (2009) measured V_{rot} and σ_g at $z = 0$ and $z = 1$ for galaxies in their simulations, and made comparisons to the observed V_{rot} and $S_{0.5} \equiv \sqrt{0.5V_{rot}^2 + \sigma_g^2}$ Tully-Fisher relations from Kassin et al. (2007). No studies have yet compared simulated galaxies to the progressive disk settling found at $0.1 < z < 1.2$ by Kassin et al. (2012).

[1] Space Telescope Science Institute, 3700 San Martin Drive, Baltimore, MD 21218, kassin@stsci.edu
[2] Department of Physics and Astronomy, Rutgers University, 136 Frelinghuysen Road, Piscataway, NJ 08854
[3] Astronomy Department, University of Washington, Box 351580, Seattle, WA 98195-1580
[4] Steward Observatory, 933 N. Cherry St., University of Arizona, Tucson, AZ 85721
[5] Astrophysics Science Division, Goddard Space Flight Center, Code 665, Greenbelt, MD 20771

In this paper, for the first time, we determine whether fully cosmological simulations of star-forming galaxies undergo the kinematic disk settling found in observations of real galaxies.

2. HYDRODYNAMIC SIMULATIONS

The kinematics of star-forming galaxies in the real universe are measured from nebular emission lines which trace gas heated in star-forming regions. In order to compare hydrodynamic simulations of galaxies most directly with observations, the simulations need to make predictions for the gas in galaxies. Treatment of the interstellar medium is crucial for this. Therefore, we look to simulations of four star-forming galaxies run with the N-Body + smooth particle hydrodynamic code GASOLINE (Wadsley, Stadel, & Quinn 2004; Stinson et al. 2006) which are described in detail in Christensen et al. (2012, 2013) and Munshi et al. (2013). They are able to match the sizes, stellar masses, bulge masses, and baryon fractions of local star-forming galaxies (Governato et al. 2007; Brook et al. 2012; Munshi et al. 2013; Christensen et al. 2013), and the size evolution of star-forming galaxies since $z = 1$ (Brooks et al. 2011). The simulated galaxies have $z = 0$ stellar masses which range $4.2 - 4.5 \times 10^{10}$ $M_\odot$ for a Kroupa, Tout, & Gilmore (1993) initial mass function (IMF). They are referred to as galaxies h239, h277, h258, and h285 in the references above.

These simulations resolve high density peaks comparable in size to giant molecular clouds. In addition, they follow the non-equilibrium formation and destruction of H_2, using a gas-phase and a dust- (and hence metallicity-) dependent scheme that traces the Lyman-Werner radiation field and allows for self-shielding by H_2 gas (Gnedin, Tassis, & Kravtsov 2009; Christensen et al. 2013). Therefore, the simulations are able to tie star formation to the presence of molecular gas, as is indicated by observations (e.g., Leroy et al. 2008; Bigiel et al. 2008; Blanc et al. 2009; Bigiel et al. 2010; Schruba et al. 2011). The efficiency of star formation is tied to the H_2 fraction, as described in Christensen et al. (2012). With the inclusion of H_2-based star formation, stars predominantly form at high densities and low temperatures (T $<$ 1000 K; see also Krumholz, Klein, & McKee 2011; Kuhlen et al. 2012). Finally, to take into account the effects of the reionization of the universe, an ultraviolet background is implemented at $z = 9$, following a modified version of the formulation by Haardt & Madau (2001).

Our simulated galaxies were chosen from lower resolution simulations to be re-simulated at high resolution based on their $z = 0$ virial masses and because they span a representative range of halo spin values and accretion histories. The re-simulations follow a 50 Mpc co-moving box around the galaxies at lower resolution than the galaxy itself. In this manner, cosmological effects are fully implemented. The re-simulations are run from $z = 150$ to $z = 0$.

The spline force softening in the high resolution region is 174 parsecs, and is kept fixed in physical parsecs since $z = 10$. In the high resolution region, dark matter particles have masses of $1.3 \times 10^5 M_\odot$, gas particles start at $2.7 \times 10^4 M_\odot$, and star particles are born with 30% of the mass of their parent gas particle, which corresponds to a maximum initial mass of $8100\, M_\odot$. Each simulated galaxy has ~ 5 million dark matter particles within its virial radius at $z = 0$ and more than 14 million total particles (dark matter, gas, and stars). Our simulations have the same mass resolution as the Eris simulation (Guedes et al. 2011), but include metal line cooling (Shen, Wadsley, & Stinson 2010) and the physics of molecular hydrogen (Christensen et al. 2012). The simulations are run for a WMAP 3 Year Cosmology: $\Omega_m = 0.24, \Lambda = 0.76, \mathrm{H_o} = 73$ km s^{-1}, $\sigma_8 = 0.77$ (Spergel et al. 2007).

2.1. *Warm & Cold Gas in the Simulations*

The nebular emission lines in real galaxies, from which internal kinematics are measured, largely come from H II regions, with a small contribution from diffuse ionized gas. Gas in H II regions has been ionized by young stars after the stars and gas emerge from their dusty birth environments inside dense regions of molecular clouds. We investigate two types of star forming gas in the simulations which should bracket the kinematic behavior of H II regions: (1) cold gas in the galaxy disks which we refer to as "cold gas", and (2) dense gas in the galaxy disks which has been heated by supernovae feedback and which we refer to as "warm gas." Cold gas is defined as having temperatures $T < 1000$K. It has typical densities of > 1 amu cm^{-3} and traces both neutral gas in the disk and molecular clouds at $\rho > 100$ amu cm^{-3} (Christensen et al. 2013). Warm gas is defined as having $\rho > 0.001$ amu cm^{-3}); it has temperatures in excess of 20,000K due to heating by feedback. Star-forming regions in observed galaxies likely contain ionized gas from both the cold and warm components because they are being observed after the young stars are visible and some feedback has had a chance to occur. Therefore, we expect the behavior of the cold and warm gas in the simulations to bracket that of HII regions.

3. KINEMATIC EVOLUTION OF SIMULATED GALAXIES

For each of the 4 simulated galaxies, we measure σ_g and V_{rot} at discrete redshifts sampling the range of observations in Kassin et al. (2012). We measure the intrinsic values of these quantities which are unaffected by observational effects such as seeing, slit width, and pixel scale. The quantity σ_g is measured as the average integrated velocity dispersion of the gas in the direction perpendicular to the disk, similar to observations. The rotation velocity V_{rot} is measured as the maximum line-of-sight velocity of the gas, also similar to the observations which use the rotation velocity on the flat part of the rotation curve. We use the actual gas particle velocities rather than circular velocities since this provides the most direct comparison to observations. Rotation velocities are all corrected for inclination.

Median values of σ_g and V_{rot} at discrete redshifts for the warm and cold gas in our 4 simulated galaxies are shown in the top panels of Figure 1. Values of these quantities for the individual simulated galaxies are shown in the bottom panels. In the top panels, the median values are compared to those for an observed mass-limited sample of 270 star-forming galaxies from Kassin et al. (2012). Qualitatively, the simulated galaxies follow the same trends as the observations: they increase in σ_g and decrease in V_{rot} with increasing redshift over $0.1 < z < 1.2$. In other words, both the simulations and the observations decrease in σ_g and increase in V_{rot} with

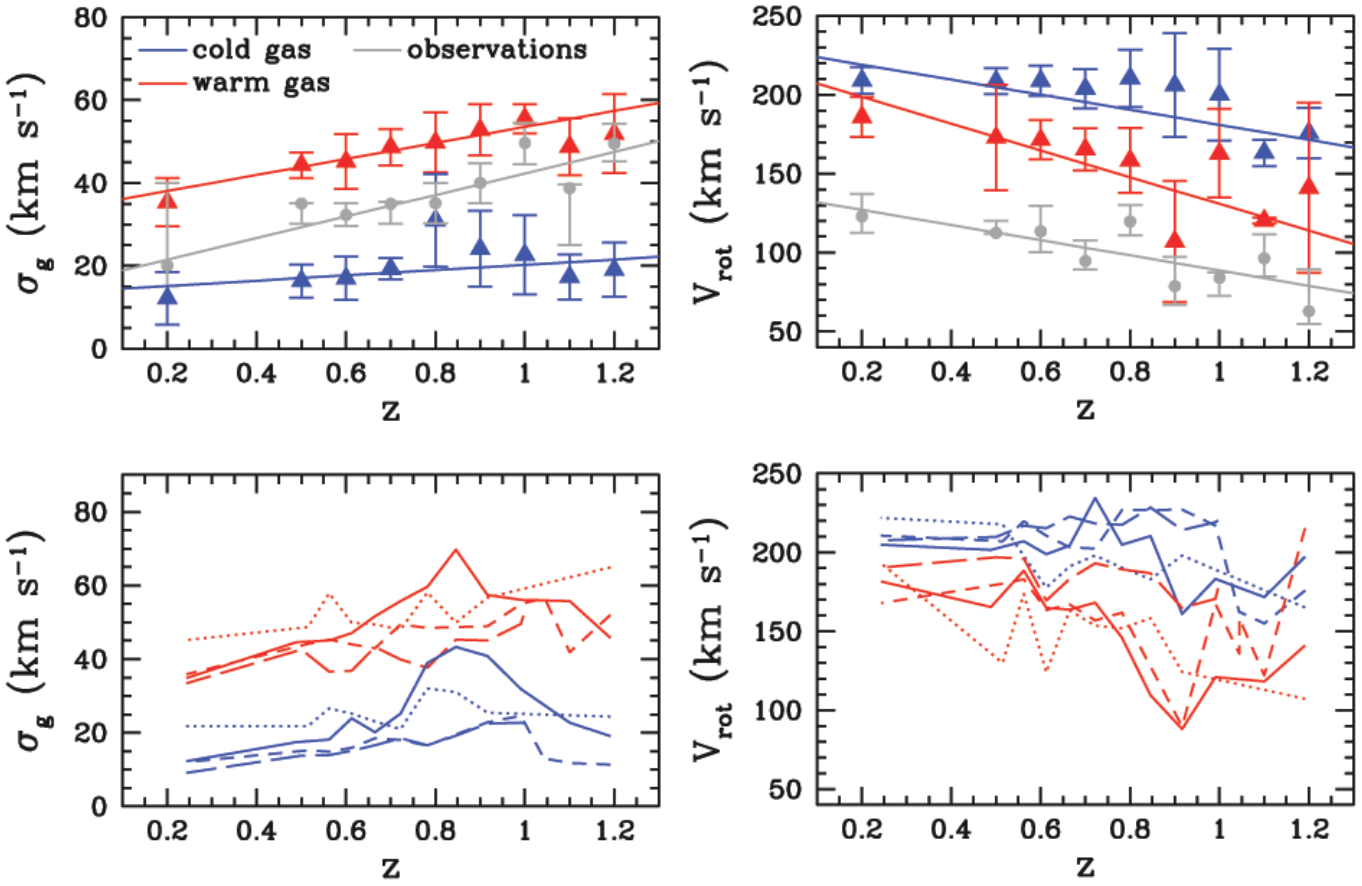

FIG. 1.— Top: The redshift evolution of the median integrated velocity dispersion σ_g and rotation velocity V_{rot} of warm and cold gas in the simulated galaxies (red and blue points, respectively) is compared with that for an observational mass-limited sample of 270 galaxies from Kassin et al. 2012 (grey points). The simulations follow the same disk settling trends as the observations: they increase in σ_g and decrease in V_{rot} with redshift (i.e., decrease in σ_g and increase in V_{rot} with time). The differences in normalizations between the simulations and observations can be attributed to differences in galaxy stellar masses for V_{rot} and temperatures/regions probed for σ_g (see text). Solid lines show linear fits given in the text. Error bars on the simulations show the rms scatter. As in Kassin et al. 2012, error bars on the observations are calculated by bootstrap re-sampling the data in each redshift bin, since their distributions are non-Gaussian. Bottom: The evolution of the warm and cold gas (red and blue lines, respectively) in the four individual simulated galaxies is shown: h285 (solid), h239 (dotted), h258 (short dashed), and h277 (long dashed). Although the simulated galaxies show the same trends as the observations in the median, individually they show significant variation with time, consistent with the large scatter of the observations.

time over the last $\sim$ 8 billion years, *demonstrating that the simulated galaxies undergo the disk settling found in observations.*

As expected, the normalizations of the simulated and observed relations differ. The median values of V_{rot} for the simulated galaxies are greater since they are more massive on average than the observed galaxies, and V_{rot} generally scales with stellar mass for disk galaxies. The masses of the simulated galaxies range $4.2 - 4.5 \times 10^{10}$ $M_\odot$ versus $6.3 - 50.1 \times 10^9$ $M_\odot$ for the observations. (The simulations and observations adopt Kroupa, Tout, & Gilmore 1993 and Chabrier 2003 IMFs, respectively, which result in consistent stellar masses.) The normalization of the σ_g versus z relations for the warm and cold gas are higher and lower than the observations, respectively. In the simulations the warm gas is affected by feedback from supernovae, which results in higher σ_g and leads to hotter temperatures compared to observed H II regions. By definition, the cold gas is cooler than observed H II regions, which results in lower σ_g.

3.1. *Quantitative Trends of σ_g and V_{rot} with Redshift*

Linear relations are fit to the median points in Figure 1 by performing least-squares fits which take into account the errors in σ_g and V_{rot} (errors in redshift are negligible). When fitting, to avoid covariances, we zero-point the medians near the middle of the samples such that they vary around $\sim$zero. We obtain the following fits for σ_g for the warm gas, cold gas, and observations, respectively:

$$\log \sigma_g - 50 = (19.3 \pm 6.2)(z - 0.6) - (4.2 \pm 1.8), \quad (1)$$

$$\log \sigma_g - 20 = (6.4 \pm 6.8)(z - 0.6) - (2.3 \pm 1.8), \quad (2)$$

$$\log \sigma_g - 35 = (26.0 \pm 5.7)(z - 0.6) - (3.1 \pm 1.4). \quad (3)$$

These fits have χ^2 values of 1.9, 2.5, and 4.7, respectively. As for the observations, the median σ_g of both the warm and cold gas grows with increasing redshift to $z = 1.2$ (i.e., decreases with time), although the relation for the cold gas is consistent with no evolution. The slopes of the relations for the warm gas and observations are consistent within uncertainties. As mentioned above, the normalization of the relations for the warm and cold gas are higher and lower than the observations, respectively.

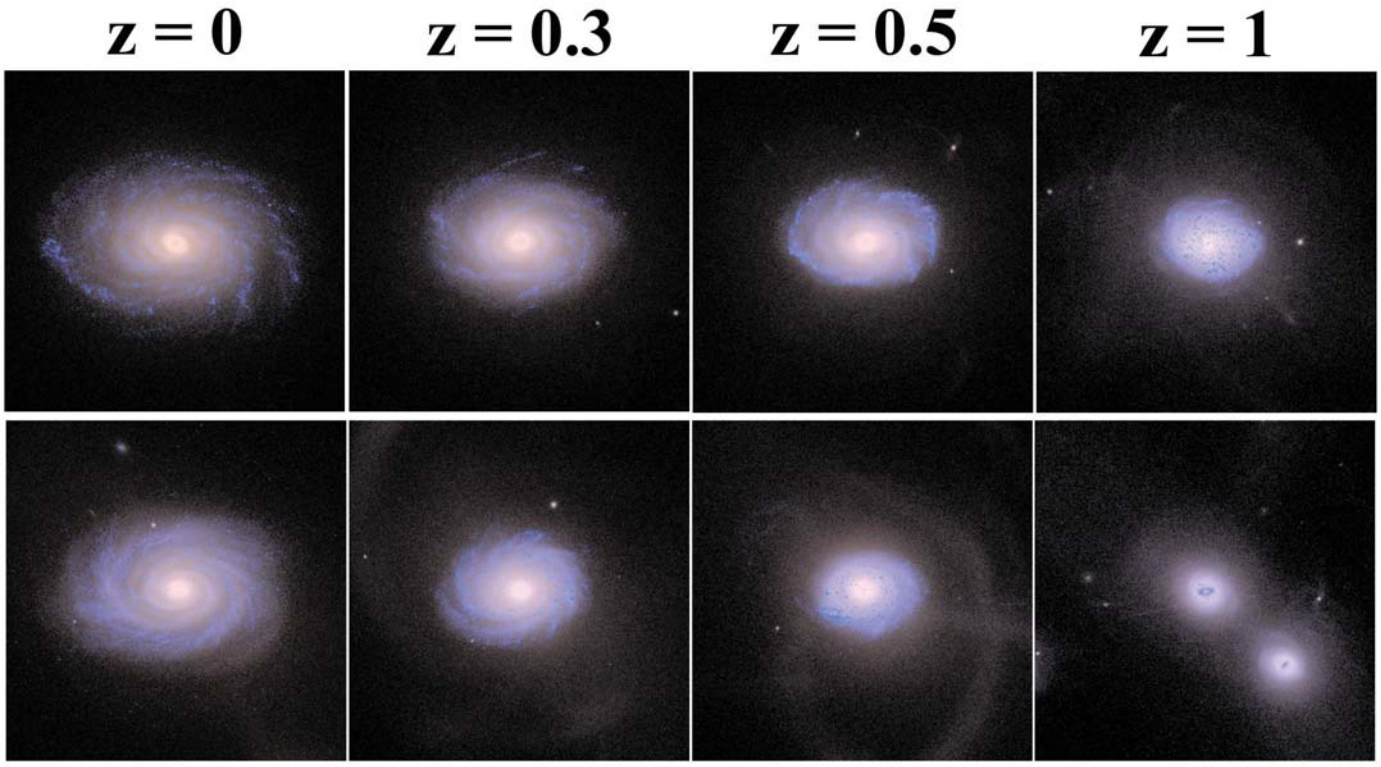

FIG. 2.— Multi-color images of two of our four simulated galaxies are shown at discrete redshifts spanning the redshift range of Figure 1. The morphologies become progressively less disturbed with time and the disk grows (from right to left), reflective of the kinematic evolution which shows disk settling with time. The images are for galaxies h277 (top panels) and h239 (bottom panels) and are combinations of g, r, and i-band images created with the `Sunrise` radiative transfer code. They are 50 kpc (physical) on a side and the central galaxy in each image is viewed at an inclination of 45°.

We obtain the following fits for V_{rot} for the warm gas, cold gas, and observations, respectively:

$$\log V_{rot} - 175 = (-84.7 \pm 11.4)(z - 0.6) - (12.0 \pm 5.5), \quad (4)$$

$$\log V_{rot} - 200 = (-47.6 \pm 11.5)(z - 0.6) - (0.1 \pm 3.8), \quad (5)$$

$$\log V_{rot} - 100 = (-48 \pm 11.5)(z - 0.6) - (7.8 \pm 3.0). \quad (6)$$

These fits have χ^2 values of 4.7, 7.4, and 9.2, respectively. As for the observations, the median V_{rot} of both the warm and cold gas decreases with increasing redshift to $z = 1.2$ (i.e., increases with time). The simulated galaxies have a higher normalization (i.e., have faster median rotation velocities) than the real galaxies, as expected because they are on average more massive than the observed galaxy sample, as discussed above.

3.2. *Kinematics and Morphology*

As is the case for real galaxies over $0.1 < z < 1.2$ (e.g., Flores et al. 2006; Kassin et al. 2007; Yang et al. 2008; Kassin et al. 2012), the kinematics of simulated galaxies are reflected in their morphologies. Images of two of our four simulated galaxies are shown in Figure 2 at discrete redshifts over the redshift range in Figure 1. Both galaxies have more disturbed morphologies at $z = 1.0$, and become progressively less disturbed with decreasing redshift. At $z = 0$ they appear as ordered disk galaxies with little disturbances or peculiarities. This morphological transformation is consistent with the kinematic settling they undergo (i.e, decrease in σ_g and increase in V_{rot} with time).

The images in Figure 2 are produced by taking into account the effects of radiative transfer and dust using a Monte-Carlo ray tracing program designed to pair with hydrodynamic simulations (`Sunrise`; (Jonsson 2006; Jonsson, Groves, & Cox 2010). In short, `Sunrise` creates a spectral energy distribution for each star particle in the simulation based on its age and metallicity, using the `Starburst99` stellar population modeling software (Leitherer et al. 1999). The metallicities of the gas particles determine how light from the galaxy is attenuated by dust, and a constant dust to gas ratio of 0.4 is assumed. The resulting images are then convolved with the SDSS g, r, and i band filters to produce those in Figure 2.

4. CONCLUSIONS

For the first time we measure the *evolution* of the kinematics of simulated star-forming galaxies over the last ~ 8 billion years, over nearly half of the age of the universe. Specifically, we measure the evolution of disordered motions (σ_g) and ordered rotation (V_{rot}) of gas in a suite of four simulated galaxies. Measurements are compared with recent observations which show the progressive settling of gas in disk galaxies over $0.1 < z < 1.2$ from disordered systems into the ordered disk galaxies common today (Kassin et al. 2012). We find that the simulated galaxies follow the same trends as the observations: they progressively decrease in disordered motions (σ_g) and increase in ordered rotation (V_{rot}) with time. Differences in normalization between the observations and simulations can be attributed to differences in the average stellar mass of the galaxy samples and gas

temperatures/regions probed.

Reproducing these observations is an important benchmark for any theory or simulation of disk galaxy formation. The observations trace the internal kinematics of star-forming galaxies over a significant period of time. Internal kinematics directly dictate how the gas in galaxies is arranged, and are strongly affected by physical processes such as feedback from star-formation, major/minor mergers, and smooth accretion of baryons. Our next step in a future work is to place constraints on the processes which have the most direct effect on disk settling.

FG acknowledges support from NSF grant AST-0607819. Resources supporting this work were provided by the NASA High-End Computing (HEC) Program through the NASA Advanced Supercomputing (NAS) Division at Ames Research Center. AB would like to thank Jay Gallagher for helpful conversations.

REFERENCES

Agertz, O., Kravtsov, A. V., Leitner, S. N., & Gnedin, N. Y. 2013, ApJ, 770, 25
Anglés-Alcázar, D., Davé, R., Özel, F., & Oppenheimer, B. D. 2013 arXiv:1303.6959
Bigiel, F. et al. 2008, AJ, 136, 2846
Bigiel, F. et al. 2010, AJ, 140, 1194
Blanc, G. A., Heiderman, A., Gebhardt, K., Evans, N. J., II, & Adams, J. 2009, ApJ, 704, 842
Brook, C. B., Stinson, G., Gibson, B. K., Wadsley, J., & Quinn, T. 2012, MNRAS, 424, 1275
Brooks, A. M. et al. 2011, ApJ, 728, 51
Ceverino, D., Dekel, A., & Bournaud, F. 2010, MNRAS, 404, 2151
Chabrier, G. 2003, PASP, 115, 763
Christensen, C., Quinn, T., Governato, F., et al. 2012, MNRAS, 425, 3058
Chistensen, C., Governato, F., Quinn, T. et al. arXiv:1211.0326
Croft, R.A. C., Di Matteo, T., Springel, V., & Hernquist, L. 2009, MNRAS, 400, 43
Flores, H., Hammer, F., Puech, M., Amram, P., & Balkowski, C. 2006, A&A, 455, 107
Förster-Schreiber, N. M., Fenzel, R., Bouché, N., et al. 2009, ApJ, 706, 1364
Gnedin, N. Y., Tassis, K., & Kravtsov, A. 2009, ApJ, 697, 55
Gnerucci, A., Marconi, A., Cresci, G., et al. 2011, A&A, 528, 88
Governato, F. et al. 2007, MNRAS, 374, 1479
Guedes, J., Callegari, S., Madau, P., & Mayer, L. 2011, ApJ, 742, 76
Haardt, F. & Madau, P. 2001, in Clusters of Galaxies and the High Redshift Universe Observed in X-rays, ed. D. M. Neumann & J. T. V. Tran
Hirschmann, M. et al. 2013, MNRAS, 436, 2929
Hopkins, P. F., Kereš, D., Murray, N. Quataert, E., & Hernquist, L. 2012, MNRAS, 427, 968
Hopkins, P. F., Kereš, D., Onorbe, J., Faucher-Giguere, C.-A., Quataert, E., Murray, N., & Bullock, J. S. arXiv:1311.2073
Jonsson, P. 2006, MNRAS, 372, 2
Jonsson, P., Froves, B. A., & Cox, T. J. 2010, MNRAS, 403, 17
Kassin, S. A., Weiner, B. J., Faber, S. M. et al., 2007, ApJL, 660, 35
Kassin, S. A., Weiner, B. J., Faber, S. M. et al., 2012, ApJ, 660, 35
Kroupa, P., Tout, C. A., & Gilmore, G. 1993, MNRAS, 262, 545
Kuhlen, M., Krumholz, M. R., Madau, P., Smith, B. D., & Wise, J. 2012, ApJ, 749, 36
Krumholz, M. R., Klein, R. I., & McKee, C. F. 2011, ApJ, 740, 74
Law, D. R., Steidel, C. C., Erb, D. K., et al. 2009, ApJ, 697, 2057
Leitherer, C., Schaerer, D., Goldader, J. D. et al. 1999, ApJS, 123, 3
Lemoine-Busserolle, M., Bunker, A., Lamareille, F., & Kissler-Patig, M. 2010, MNRAS, 401, 1657
Lemoine-Busserolle, M. & Lamareille, F. 2010, MNRAS, 402, 2291
Leroy, A. K. et al. 2008, AJ, 136, 2782
Mayer, L. et al. 2001, ApJ, 559, 754
McCarthy, I. G., Schaye, J., Font, A. S., Theuns, T., Frenk, C. S., Crain, R. A.,& Dalla Vecchia, C. 2012, MNRAS, 427, 379
Munshi, F., Governato, F., Brooks, A. M. et al. 2013, ApJ, 766, 56
Quinn, T., Katz, N., & Efstathiou, G. 1996, MNRAS, 278, L49
Rôskar, Teyssier, Agertz, Wetzstein, & Moore arXiv:1308.6321
Schruba, A. et al. 2011, AJ, 142, 37
Shen, S., Wadsley, J., & Stinson, G. 2010, MNRAS, 407, 1581
Spergel, D. N. et al. 2007, ApJS, 170, 377
Stinson, G., Seth, A., Katz, N. et al. 2006, MNRAS, 373, 1074
Stinson, G., Brook, C., Macciò, A. V., Wadsley, J., Quinn, T. R., & Couchman, H. M. P. 2013, MNRAS, 428, 129
Vergani, D. et al. 2012, A&A, 546, 118
Vogelsberger, M., Genel, S., Sijacki, D., Torrey, P., Springel, V., & Hernquist, L. 2013, MNRAS, 436, 3031
Wadsley, J. W., Stadel, J., & Quinn, T. 2004, New Astronomy, 9, 137
Wise, J. H., Abel, T., Turk, M. J., Norman, M. L., & Smith, B. D. 2012, MNRAS, 427, 311
Wright, S., Larkin, J. E., Law, D. R. et al. 2009, ApJ, 699, 421
Yang, Y. et al. 2008, A&A, 477, 789
Zemp, M., Gnedin, O. Y., Gnedin, N. Y., & Kravtsov, A. V. 2013, ApJ, 748, 54